Studies of Electron Temperature Fluctuations in the Core of Alcator C-Mod Plasmas via Correlation Electron Cyclotron Emission

by

Curran Y. M. Oi

Submitted to the Department of Nuclear Science and Engineering
in partial fulfillment of the requirements for the degree of

Bachelor of Science in Nuclear Science and Engineering

at the

MASSACHUSETTS INSTITUTE OF TECHNOLOGY

June 2013

Author .....
Department of Nuclear Science and Engineering
January 30, 2013

Certified by .....
Anne E. White
Assistant Professor of Nuclear Science and Engineering
Thesis Supervisor

Accepted by .....
Dennis Whyte
Professor of Nuclear Science and Engineering
Chair, NSE Committee for Undergraduate Students

Studies of Electron Temperature Fluctuations in the Core of Alcator C-Mod Plasmas via Correlation Electron Cyclotron Emission

by

Curran Y. M. Oi

Submitted to the Department of Nuclear Science and Engineering
on January 30, 2013, in partial fulfillment of the
requirements for the degree of
Bachelor of Science in Nuclear Science and Engineering

Abstract

Transport in tokamak plasmas is higher than predicted by neoclassical theory; this anomalous transport is believed to be attributed to turbulent fluctuations. New Correlation Electron Cyclotron Emission (CECE) experiments on Alcator C-Mod show lower levels of electron temperature fluctuations in the saturated ohmic confinement (SOC) regime than in the linear ohmic confinement (LOC) regime, however the line-averaged density fluctuation data collected from ohmic plasmas previously showed the opposite trends. The apparent contradiction is explained by a change in the dominant turbulence modes in each confinement regime. Linear stability analysis shows that the LOC regime is dominated by trapped electron mode (TEM) turbulence and the SOC regime is on the border between the ion temperature gradient (ITG) and TEM turbulence modes being dominant. It is reasonable to believe that the TEM turbulence mode drives electron temperature fluctuations, which explains the higher electron temperature fluctuation levels seen in the LOC regime compared to the SOC regime.

Thesis Supervisor: Anne E. White
Title: Assistant Professor of Nuclear Science and Engineering

Acknowledgments

I would like to thank Professor Anne White and graduate student Choongki Sung for guiding me through my research, helping me develop a foundational understanding of plasma physics and experimental research, and for providing extensive assistance in writing this thesis.

Contents

List of Figures

List of Tables

1. Introduction

With ITER (International Thermonuclear Experimental Reactor) under construction in France, it is increasingly important in plasma physics to have a well-characterized model for turbulence in fusion plasmas. In ITER the ion and electron temperatures will be comparable [1] and electron transport will dominate, so it is crucial to understand electron-driven turbulence modes in detail.

Presently, the electron heat conductivity in fusion plasmas is higher than predicted by neoclassical theory [2, p.497] and it is important to investigate the cause of the discrepancy. A key part of the turbulence model is understanding which turbulence modes are dominant in different plasma regimes; the change in dominant turbulence modes with confinement regime is not well understood. One example is the change in dominant turbulence modes between the linear ohmic confinement (LOC) and saturated ohmic confinement (SOC) regimes. Figure 1-1 shows confinement time as a function of line averaged electron density, $<n_e>$ for Alcator C-Mod. The LOC regime on the left of the plot is characterized by a linear increase in confinement time, τ_e, with $<n_e>$, while the SOC regime occurs when that effect saturates, when there is no longer an increase in τ_e with $<n_e>$.

While ITER will not run ohmic plasmas because it will be dominant alpha particle heated [1], understanding more about what factors drive the transition from the dominance of one turbulence mode to another during a change in confinement regime will improve understanding of underlying connections between various plasma parameters, dominant turbulence modes, and transport. Generally trapped electron mode (TEM) and ion temperature gradient (ITG) turbulence modes are both unstable and electron heat transport is associated with both [4], so it is difficult to separate the

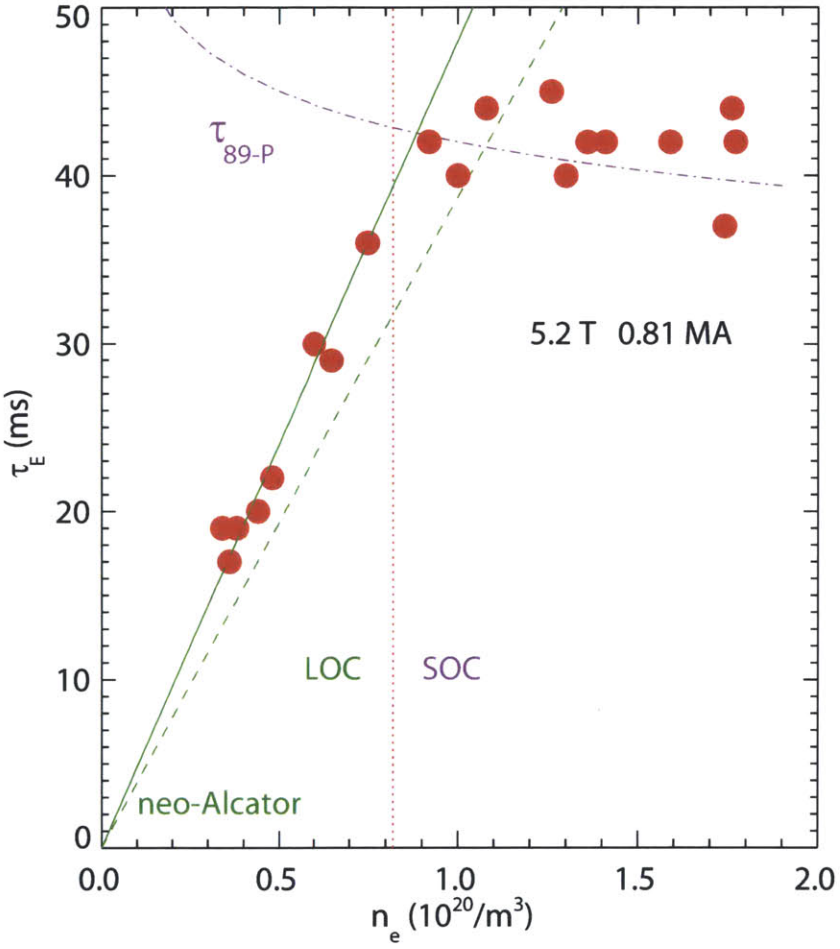

Figure 1-1: Plot of line averaged electron density, $<n_e>$, against confinement time, τ_e for Alcator C-Mod. The points on the left of the graph correspond to the linear ohmic confinment (LOC) regime, while those on the right correspond to the saturated ohmic confinement regime (SOC). The transition occurs at about $0.8 \times 10^{20}/\mathrm{m}^3$. The shots used in this plot were run at a magnetic field $B_T = 5.2\mathrm{T}$ and a plasma current $I_P = 0.81\mathrm{MA}$. This figure was adapted from [3].

Table 1.1: Summary of Data in Primary Literature

Ref	Author	Year	TEM → LOC and ITG → SOC	Fluctuation Data	Growth Rates
[5]	Angioni	2005	Yes	No	No
[6]	Esposito	2004	Yes	No	No
[7]	Lin	2009	No	Yes	Yes
[8]	Rettig	2001	Yes	Yes	Yes
[3]	Rice	2011	Yes	Yes	No

effects of TEMs and ITGs in plasmas. By investigating the change in turbulence modes with changes in confinement it may be possible to shed light on the cause of the anomalous transport seen in plasmas, which might be explained by turbulent fluctuations [2, p.498]. There is a general agreement among plasma physicists that LOC plasmas are dominated by TEM turbulence and SOC plasmas are dominated by ITG turbulence [3].

Table 1 gives an overview of the primary literature concerning dominant turbulence modes in LOC and SOC plasmas. The most notable fact about the table is that only the Rettig (2001) paper supports the common stance about the LOC regime being TEM dominated and the SOC regime being ITG mode dominated with both fluctuation data and linear growth rate calculations.

Experiments conducted on the ASDEX Upgrade tokamak in Germany and published in 2005 present evidence that LOC regimes are dominated by TEM turbulence and SOC regimes are ITG dominated. The results presented suggest that this connection between confinement regimes and turbulence modes can be explained by a change in the density profile of the plasma with the application of electron cyclotron heating (ECH). When ECH was applied to LOC plasmas, the density profile flattened, as it should, if the transport is dominated by TEM turbulence [5]. The paper presents no linear stability analysis and presents no fluctuation data, which would both work to strengthen its argument. Given that this is the case, the fact that the density profile flattens when ECH is applied is not sufficient to prove that LOC modes are TEM dominant.

Results similar to those from the ASDEX Upgrade have also been presented by

experimentalists working at the Frascati Tokamak Upgrade (FTU) tokamak in Italy [6]. The evidence for LOC corresponding to TEM dominated turbulence and SOC mode being dominated by ITG turbulence is the fact that ion heat diffusivity increases and electron heat diffusivity decreases as density increases and the ion heat diffusivity is higher than the electron heat diffusivity in SOC plasmas [6]. In addition, they turn to theory, which suggests that ITG modes should be suppressed with density peaking [6]. No linear stability or fluctuation analysis is presented to support the argument for the connection between confinement regime and dominant turbulence mode [6].

Recent results from Alcator C-Mod at MIT have shown fluctuation data relating to the LOC/SOC transition, showing higher relative density fluctuations in the SOC regime relative to the LOC regime [7]. The paper does not make a claim as to whether the LOC regime is TEM dominated or the SOC regime is ITG dominated. It says only that the significance of the ITG mode increases with density in the SOC regime [7].

GYRO simulations used for linear stability analysis have shown that for LOC plasmas tested at Alcator C-Mod the growth rate for the ITG mode was larger than the growth rate of the TEMs, suggesting that the thermal transport due to ITG modes is higher than that due to TEMs [7]. This analysis was done for $k_\theta \rho_s \sim 0.8$, where k_θ is the poloidal wavenumber and $\rho_s = c_s/\Omega_i$. ρ_s is the ion sound gyroradius, c_s is the sound speed, and Ω_i is the ion gyrofrequency [9]. Here, it is notable that the ion temperature gradient was estimated using a D-D neutron measurement and was not directly measured [7]. Results from Alcator C-Mod in 2011 also suggest that the LOC regime is dominated by TEMs and the SOC regime is ITG dominated [3]. The fluctuation data presented claims that the density fluctuations with $2\text{cm}^{-1} \leq k_\theta \leq 11\text{cm}^{-1}$ and frequencies above 70 kHz decrease sharply when the plasma reverses rotation from the cocurrent to countercurrent direction [3]. This rotation change is correlated to the transition from LOC to SOC.

A 2001 paper by Rettig may be the only published source that claims the LOC regime is TEM dominated and the SOC regime ITG dominated while also providing fluctuation data and linear stability analysis [8]. The experimental results come

from the DIII-D tokamak in San Diego, where the value of $k_\theta \rho_s$ probed with density fluctuation measurements was between 0.1 and 0.5. The relative density fluctuation level was determined to be higher for SOC plasmas than for LOC plasmas.

The Rettig paper also gives the growth rates of the ITG mode for LOC and SOC plasmas as a function of minor radius. These plots also show the E×B shear rate in the LOC and SOC plasmas as a function of minor radius, and it can be seen that the E×B shearing rate is in competition with the growth rate of the ITG mode in the LOC plasmas, whereas the ITG growth rate is higher than the corresponding E×B shearing rate for the SOC plasmas [8]. This indicates that the ITG mode cannot drive transport in the LOC regime, and it can in the SOC regime. This supports the claim that SOC plasmas are ITG dominated.

The research presented in this thesis aims to use newly available local electron temperature fluctuation data from LOC and SOC plasmas at Alcator C-Mod to shed light on the turbulence characteristics in the LOC and SOC regimes. The local electron temperature fluctuation data were collected using the CECE (correlation electron cyclotron emission) diagnostic installed at Alcator C-Mod at MIT. This fluctuation data set will be accompanied by linear stability analysis for both SOC and LOC plasmas. This analysis differs from the past results in that it focuses on electron temperature fluctuations, and the fluctuations characterized by the other papers were all density fluctuations. No other papers have published temperature fluctuation measurements in their analysis of LOC and SOC plasmas so this research will be valuable to the scientific community. The setup of the diagnostics at Alcator C-Mod also allows the turbulence team to make simultaneous measurements of density profiles and density fluctuations.

The objective of this study will be investigating the change in electron temperature fluctuation characteristics between the LOC and SOC regimes. Part of the analysis indicates that LOC plasmas are dominated by trapped electron mode (TEM) turbulence and SOC plasmas are dominated by ion temperature gradient (ITG) turbulence. The relationship between the shift in confinement regime and the shift in dominant turbulence mode with respect to electron temperature fluctuation levels will be a

clear topic of analysis and discussion in this study. This thesis will describe the new CECE diagnostic recently installed at Alcator C-Mod, which is used to collect local long wavelength broadband temperature fluctuation measurements in fusion plasmas. This first section acts as a background and motivation for studying CECE and the turbulence characteristics of the LOC/SOC regimes. Section 2 explains how a tokamak operates. Section 3 is an overview of how the CECE diagnostic operates, and includes the general principles of ECE and how the diagnostic extracts data from the plasma. Section 4 is an overview of the hardware used in the CECE diagnostic. Section 5 presents the data and results of the research conducted for this thesis. The sixth and final section presents the conclusions of the thesis and gives suggestions for future work on the project.

2. Tokamaks

A tokamak is a toroidal machine built for the purpose of conducting nuclear fusion experiments. The fuel is heated to tens of millions of degrees Kelvin (1-10 keV) [10], at which point it is completely ionized. The fuel is then a plasma and can be contained in the tokamak using magnetic fields. At these high temperatures nuclear fusion occurs. A cross section of the Alcator C-Mod tokamak at MIT is given in Figure 2-1. The following sections will outline the important parameters in a tokamak.

2.1 Lawson Criterion

The goal of fusion research on tokamaks is to achieve a point in operation where the power generated by the fusion reaction is greater than the power used to heat the plasma. The minimum condition for reaching this point in tokamaks is called the Lawson criterion, which requires:

$$n\tau_E > 10^{20} m^{-3} s \tag{2.1}$$

where n is the plasma density and τ_E is the energy confinement time [10]. This parameter, as well as those that follow, are designed with a deuterium-tritium (D-T) fusion reaction in mind [10]. The energy confinement time τ_E is defined as a function of W, the global plasma energy content, and P, the total applied heating power [10]:

$$\tau_E = \frac{W}{P - \frac{dW}{dt}} \tag{2.2}$$

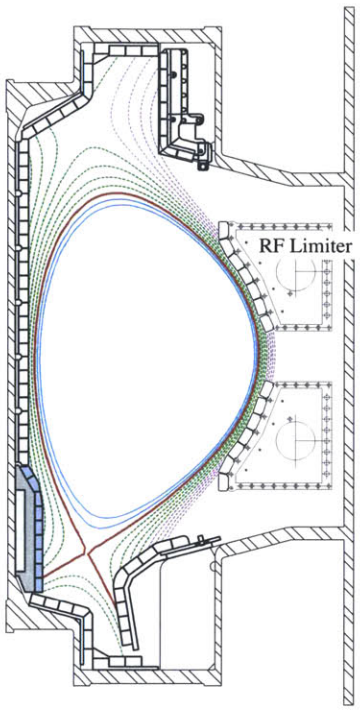

Figure 2-1: Cross section of the Alcator C-Mod tokamak. Adapted from [11, p.1-12].

During the fusion process, α particles are produced. While contained in the magnetic field of the tokamak, these α particles are capable of providing heating to the plasma [10]. The power density provided by α particle heating is:

$$P_\alpha = \frac{1}{4} n^2 < \sigma v > \varepsilon_\alpha \tag{2.3}$$

where n represents the deuterium and tritium density without impurities, which are equal, $< \sigma v >$ is the Maxwellian averaged fusion rate coefficient, and ε_α is the energy of the α particle, $\sim$3.5 MeV [10]. The power density losses of the system are given by:

$$P_L = \frac{3nT}{\tau_E} \tag{2.4}$$

If the plasma is heated to a sufficiently high temperature, around 4.4 keV [2, p.65], the minimum value required for the ignition of the plasma is reached [10, p.2-25]. The fusion parameter $p\tau_E$, where p is pressure and τ_E is energy confinement time, is minimized when the temperature is 15 keV, the pressure is about 8 atm and the

confinement time is approximately 1s [2, p.67]. Ignition occurs when $P_\alpha > P_L$ [10, p.2-25]. This value corresponds to about 1.5 or 2 times the Lawson criterion put forth in equation (2.1) [10, p.2-25]. Physically this means that the heating provided by the alpha particles in the plasma is greater than or equal to the power losses, meaning the plasma is self-heated and the outside heating systems can be turned off, while the fusion process continues [10, p.2-25].

2.2 Magnetic Confinement

The fuel used in tokamaks exists at very high temperatures during operation. At these high temperatures the fuel ionizes, becoming plasma. Powerful magnetic fields are used to confine the plasma to the shape of the toroid [12]. These magnetic fields take advantage of the charged nature of plasma and the Lorentz force [12]:

$$\vec{F}_{Lorentz} = q(\vec{E} + \vec{v} \times \vec{B}) \tag{2.5}$$

where q is the charge of a particle, E is the electric field, v is the particle velocity, and B is the magnetic field [12].

This force causes the electrons and ions in the plasma to gyrate in a helical formation around the toroidal magnetic field lines inside the tokamak [12].

This magnetic field confines the plasma and reaches several Tesla in current machines [10, p.2-25]. Though the toroidal magnetic field is the strongest magnetic field required to confine the plasma, a tokamak also requires a poloidal magnetic field, which acts in the plane of a cross section of the tokamak, and a vertical magnetic field [10, p.2-25]. This poloidal field is produced by the plasma current in the tokamak and is smaller than the toroidal magnetic field by about an order of magnitude [10, p.2-25].

Because the density is on the order of 10^{20} particles/m^3, which is approximately 10^{-5} the particle density of the atmosphere, the plasma in the tokamak is required to be enclosed in a vacuum chamber [10, p.2-25].

2.3 Heating

With the goal of achieving ignition in tokamak fusion devices, various forms of heating have been developed. A few of the primary methods are described in this section, including ohmic heating and the different forms of radio frequency heating [10, p.114-133].

2.3.1 Ohmic Heating

The initial heating in a tokamak used during startup of the device is ohmic heating [10, p.114-133]. This comes from the toroidal current generated when the current in the central solenoid is ramped up. This method is useful for achieving temperatures up to about 1keV but the residual gains of turning up ohmic heating power further drops off quickly [10, p.114-133]. This is due to the fact that collisionality decreases with the increasing temperature, meaning that the plasma has a reduced resistance [10, p.114-133]. At this point other methods of heating must be used to push the plasma temperature closer to the 10keV or higher temperature required for ignition.

2.3.2 Radio frequency (RF) Heating

In order to provide extra heating to the plasma, electromagnetic waves are injected into the tokamak [10, p.114-133]. The electric field of the wave accelerates the charged particles in the plasma, increasing their velocity and causing the plasma to heat up via collisions [10, p.114-133]. Electron cyclotron, ion cyclotron, and lower hybrid heating are examples of this method used in tokamaks. The general formula for the resonant frequency of a charged particle in a tokamak is:

$$f_{ec,n} = \frac{nqB}{2\pi\gamma m} \tag{2.6}$$

where n is the harmonic number, q is the charge of the particle, B is the magnetic field, γ is the Lorentz factor, and m is the rest mass of the particle [12].

Electron cyclotron resonance heating (ECH) applies the principles of radio fre-

quency heating to electrons. When the fuel in a tokamak is in its ionized form, there are many electrons in the plasma gyrating around the toroidal magnetic field line and these electrons have a characteristic resonance frequency that scales linearly with the applied toroidal magnetic field [10]. Electromagnetic waves with this frequency are injected into the plasma and drive the electrons at their resonant frequency, increasing the plasma temperature [10, p.114-133].

The principle applied to ion cyclotron resonance heating (ICRH) is the same as with ECH, except the waves injected into the plasma have a different frequency because the resonant frequency of the particles is inversely proportional to their mass [10, p.114-133]. Thus the waves used in ICRH have frequencies lower than those used for ECH by the mass ratio [10, p.114-133]. For example, the deuteron to electron mass ratio is about 3600, and the ICRH frequency used is less than 100MHz, while the frequency used for ECH is less than 300GHz [2, p.536].

Lower hybrid heating uses electromagnetic waves with frequencies between the electron and ion cyclotron resonant frequencies [12]. For waves with these frequencies the index of refraction for the plasma is large, meaning that the wave is reflected by the plasma and cannot heat it directly [12]. Thus it is necessary for a slow wave to tunnel through the edge plasma; it is then absorbed at the lower hybrid resonance [10, p.114-133] and heats the plasma.

2.4 Fuel Sources

Tokamaks are designed to run primarily using the deuterium-tritium (D-T) fusion reaction. The D-T reaction is very good energetically, with each D-T fusion event releasing 17.6 MeV of energy [10, p.114-133]:

$$D + T \rightarrow \alpha + n + 17.6MeV \tag{2.7}$$

This energy is shared between the α particle, which receives about 3.5 MeV of energy and the neutron, n, which gets the other 14.1 MeV [10, p.114-133]. In addition to

using the fuel injected into the reactor at the start of operation, tokamaks have the potential to utilize breeder reactions [10, p.114-133].

Fuel breeding in tokamaks would involve a blanket consisting of mostly lithium placed between the plasma and the containment vessel. It will absorb the energy of the 14MeV neutrons produced in the fusion reaction, transferring the energy to a coolant, and act as a tritium breeder [10, p.114-133]. This second functionality, as a tritium breeder, is important due to the fact that tritium is not found naturally on earth because it has a half-life of 12.3 years [10, p.114-133]. In order to continually have a supply of tritium for the D-T fusion reaction it makes sense to have a breeder reaction, which the lithium blanket can provide via reactions with neutrons [10, p.114-133]:

$$^{6}_{3}Li + n \rightarrow \alpha + T + 4.8MeV \tag{2.8}$$

$$^{7}_{3}Li + n \rightarrow \alpha + T + n - 2.5MeV \tag{2.9}$$

Since the neutrons incident on the blanket have about 14MeV of energy, both equation (2.8) and equation (2.9) can occur [10, p.114-133]. These processes enable continuous tritium production during operation of the tokamak.

3. Electron Cyclotron Emission and Correlation Methods

3.1 Electron Cyclotron Emission (ECE)

As stated in section 1, it is believed that turbulent fluctuations are responsible for anomalous transport seen in fusion plasmas, which limits the achievable τ_e and limits attainment of ignition in devices smaller than ITER [2, p.498]. Electron cyclotron emission (ECE) and correlation ECE (CECE) diagnostics exploit the radiation emitted by electrons in their gyrating orbits around the magnetic field lines in a tokamak in order to measure the electron temperature and associated turbulent fluctuations in fusion plasmas [13, p.175-179]. The electrons and ions in the plasma emit radiation due to the fact that they are charged particles and they accelerate due to the circular motion they maintain around the toroidal magnetic field lines.

ECE diagnostics are typically used to measure electron temperature by observing the second harmonic ECE given by equation (3.1),

$$f_{ec,n} = \frac{nqB}{2\pi\gamma m} \tag{3.1}$$

where n is the harmonic number, q is the charge of the particle, B is the magnetic field, γ is the Lorentz factor, and m is the rest mass of the particle. The radiation observed is the second harmonic X-mode radiation, which is chosen because the plasma acts like a blackbody for this emission [11, p.1-12]. The second harmonic is preferable to the first because it is more accessible due to its higher frequency [11, p.1-12]. X-mode

refers to the polarization of the radiation, which is polarized perpendicular to the magnetic field lines in the tokamak. O-mode radiation is polarized parallel to the magnetic field lines in the tokamak [11, p.1-12].

It is possible to use Plancks equation to see that the plasma emits radiation like a blackbody at the first and second harmonics of ECE. Plancks equation is given by equation (3.2)

$$I(f) \approx B(f) = (\frac{hf^3}{c^2})\frac{1}{exp(hf/kT) - 1} \tag{3.2}$$

where h is Plancks constant, f is the frequency of the radiation, c is the speed of light, k is Boltzmanns constant, and T is the temperature of the plasma [14, p.22]. In fusion plasmas $hf << kT$. Under this condition, equation (3.2) reduces to equation (3.3).

$$I(f) \approx \frac{f^2 kT}{c^2} \tag{3.3}$$

Equation (3.3) shows that the intensity of the emitted radiation is proportional to the temperature of the plasma, which means the plasma volume can be approximated as a blackbody. This makes the second harmonic X-mode ECE a good harmonic to observe via CECE [11, p.1-12].

The magnetic field in a tokamak is proportional to 1/R and the second harmonic ECE falls above the various other resonance and cutoff frequencies in the plasmas, as shown in Figure 3-1.

The lower sensitivity limit of the ECE diagnostic is set by the thermal noise of the signal [15], which is typically about 5% of the amplitude of the signal [16]. The thermal noise therefore masks the underlying turbulent fluctuations, which have a magnitude closer to 1% [17]. The sensitivity of the diagnostic can be improved by correlating two signals using standard signals techniques.

There are a few different ways to perform CECE: spatial decorrelation, spectral decorrelation, disjoint volumes, and autocorrelation [16]. The two primary methods of interest are the first two, and the CECE diagnostic at Alcator C-Mod uses the spectral decorrelation technique [17].

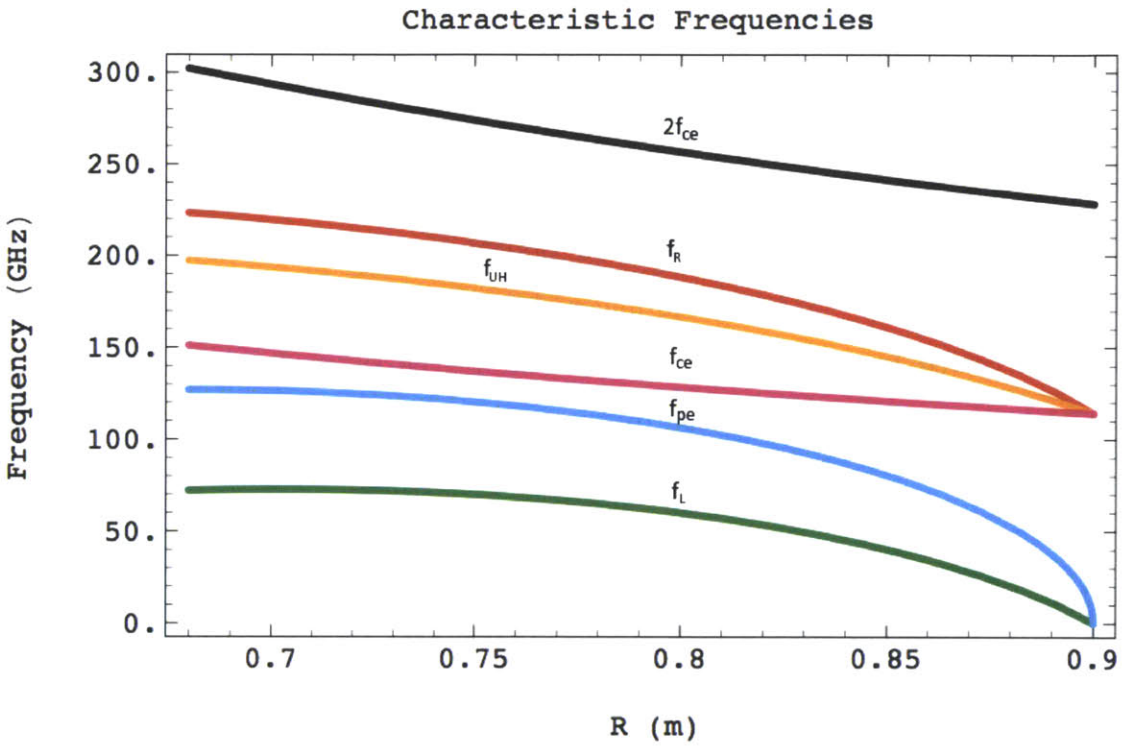

Figure 3-1: Cutoff, resonance, plasma, and cyclotron frequencies for C-Mod plasmas using the cold plasma approximation. Adapted from [11, p.1-12]. Magnetic field on axis used to produce this figure is about $B_t \sim 5.4$T.

3.2 Correlation Electron Cyclotron Emission (CECE)

3.2.1 Spatial Decorrelation

Spatial decorrelation relies on the use of two radiometers aimed at the same location in the plasma. There must be some angular separation of the antennas, which is dictated by equation (3.4):

$$\theta_{min} \approx \frac{D_C}{\lambda} = \frac{D}{L} \tag{3.4}$$

where θ_{min} is the minimum angular separation of the radiometers, D_C is the noise correlation length, λ is the electron cyclotron wavelength, D is the separation between the radiometers, and L is the distance between the radiometers and the volume of plasma they are aimed at [16]. This method hinges on the understanding that the thermal noise in the two signals in uncorrelated and therefore correlation of the two signals received by the radiometers can remove the thermal noise and reveal the underlying turbulent fluctuations [16].

3.2.2 Spectral Decorrelation

Spectral decorrelation is another method that can be used to correlate ECE signals to increase their sensitivity to turbulent fluctuations. This method relies on a similar assumption to that made in the spatial decorrelation method, namely that two signals coming from the same plasma volume which are separated in frequency space have uncorrelated thermal noise [16]. In this technique, only one radiometer is aimed at the plasma, making the setup much easier than for the spatial decorrelation technique. The signal collected from the plasma is separated using band pass filters to obtain signals in similar but non-overlapping parts of frequency space. The sensitivity of the CECE diagnostic when the spectral decorrelation technique is used is given by equation (3.5) [2,3].

$$(\frac{\tilde{T}_e^{min}}{\bar{T}_e})^2 > \frac{2B_{vid}}{\sqrt{N}B_{IF}} \tag{3.5}$$

where T_e is the electron temperature, B_{vid} is the video bandwidth, B_{IF} is the bandwidth of the intermediate frequency (IF) section of the CECE diagnostic, and N is the number of data points ($N = 2B_{vid}\Delta t$, where Δt is the length of time used to collect data) [15].

3.2.3 Correlation of the two signals

The radiation emitted by the plasma can be considered to be blackbody radiation [16]. Its intensity can be expressed as an average value and a fluctuating component, as given in equation (3.6).

$$I(t) =< I(t) > +i(t) \tag{3.6}$$

where $i(t)$ is the fluctuating component of the intensity. The fluctuating components of the intensity of the radiation contain information about the turbulent fluctuations and the thermal noise of the system. By cross-correlation of the two signals obtained either via spatial or spectral decorrelation techniques, it is possible to reduce the thermal noise terms in the signal. The two signals can be represented as being comprised of a fluctuating temperature component and a fluctuating noise component, as in equation (3.7) and equation (3.8).

$$S_1 = \tilde{T} + \tilde{N}_1 \tag{3.7}$$

$$S_2 = \tilde{T} + \tilde{N}_2 \tag{3.8}$$

The correlation of the two signals in equations (3.7) and (3.8) is given by equation (3.9) [16].

$$< S_1 S_2 >=< \tilde{T}^2 > + < \tilde{N}_1 \tilde{N}_2 > + < \tilde{T}\tilde{N}_1 > + < \tilde{T}\tilde{N}_2 > \approx < \tilde{T}^2 > \tag{3.9}$$

where the signals S_1 and S_2 are comprised of the fluctuations due to noise and those due to temperature. This method is typically carried out in Fourier space and it

reveals the underlying electron temperature fluctuations, expressed as a cross-power spectrum [16].

4. CECE Hardware

The CECE hardware consists of three discrete systems: the in-vessel optics, the radio frequency receiver, and the intermediate frequency system. The in-vessel optics collect the radiation emitted by the plasma, the receiver down-mixes the signal coming from the plasma and sends it to the intermediate frequency section, which removes the equilibrium component of the signal and separates it in frequency space. The signal is then recorded by the digitizer and can be analyzed by IDL post-processing codes.

4.1 Optics System

A diagram of the optics system is shown in Figure 4-1. The in-vessel components are shown in the left, consisting of the parabolic and flat mirror. The ex-vessel components consist of a lens to collimate the beam of radiation and a horn antenna, which leads to the RF section.

4.1.1 In-vessel components

The in-vessel optics system consists of a parabolic and a flat mirror, which collect the radiation from the plasma and send it to the receiver. The in-vessel optics as they

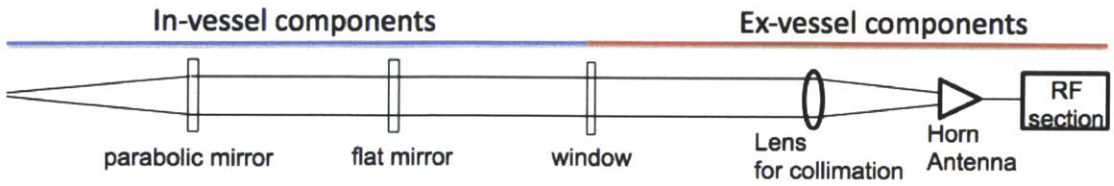

Figure 4-1: Diagram of CECE optics system (not to scale)

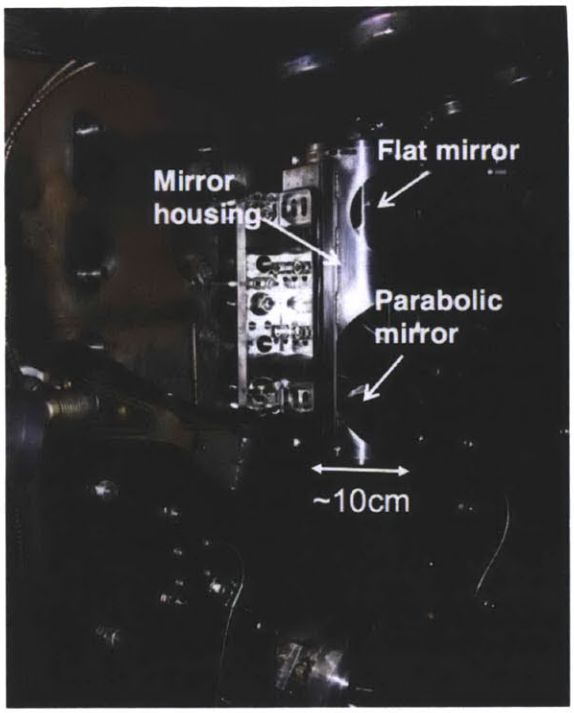

Figure 4-2: In-vessel optics components. The flat and parabolic mirrors are contained in the mirror housing. The two mirrors focus the radiation from the plasma and direct it to the CECE hardware.

look inside the tokamak can be seen in Figure 4-2.

The mirrors, horn antenna, and lens system determine the diameter of the beam of radiation. The ECE radiation emitted by the plasmas in a tokamak follows the principles of Gaussian optics, meaning that beams of smaller diameter spread more rapidly. It is important, therefore to optimize the configuration of the parabolic and flat mirror, along with the ex-vessel lens to minimize the spot size in the plasma. Having a small spot size means the CECE diagnostic is capable of measuring the turbulent electron temperature fluctuations in the plasma. Figure 4-3 shows how the diameter of the Gaussian beam changes as it passes from the plasma, to the mirror, and through the lens.

4.1.2 Ex-vessel components

After the beam of radiation reflects off the mirrors and passes through the window it is incident upon the collimating lens at the front of the receiver. Depending on the

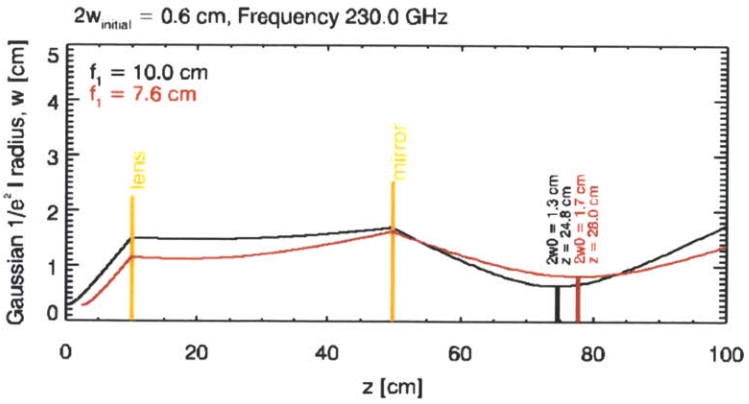

Figure 4-3: Beam diameter mapped from the plasma (>50cm) through the mirror system (<50cm and >10cm) and to the lens and electronics systems (<10cm).

lens used for the collimation of the radiation, the CECE radiometer is able to probe the plasma to different values of ρ: by decreasing the focal length of the lens, the radiometer can see further inside the plasma. This comes at the cost of the beam diameter however; the minimum beam diameter increases as the focal length of the lens is decreased. This relationship is shown in Figure 4-4 and is one of the challenges facing the CECE diagnostic: the parabolic and flat mirrors, along with the ex-vessel lens on the radiometer, will need to be adjusted in order for the radiometer to measure electron temperature fluctuations closer to the core of the plasmas, which occur at ρ =0.5.

4.2 CECE Receiver (RF section)

The CECE receiver is mounted outside the tokamak, though it is placed as close as possible to the tokamak in order to reduce losses in the signal between the tokamak and the receiver. Figure 4-5 shows the receiver as it appears mounted against the side of the Alcator C-Mod tokamak. The receiver collects the radiation from the plasma when it has a frequency of about 250 GHz. This corresponds to millimeter wavelengths, which are downconverted in the RF front-end electronics.

The diagram of the RF and IF hardware systems of the radiometer are shown in Figure 4-6. The RF section has a horn antenna that receives the signal, which

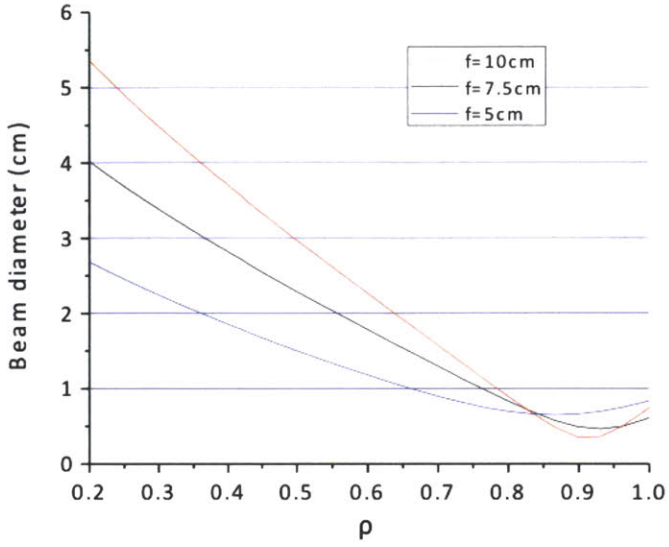

Figure 4-4: Beam diameter given as a function of the normalized radius ρ for different ex-vessel lenses. The minimum beam diameter for all three lenses shown occurs for ρ between 0.8 and 1.0. The three lenses are defined by their focal lengths, given in the legend as 10cm, 7.5cm, and 5cm.

is passed to a band pass filter that selects the range of frequencies corresponding to the second harmonic ECE radiation. A sub-harmonic mixer shifts the signal to the 2-18 GHz frequency range, which falls in the intermediate frequency (IF) range. The signal is then passed to the IF section.

4.3 CECE IF section

As shown in Figure 4-6, after the signal is down-mixed to the intermediate frequency range it enters the IF section of the hardware. In the IF section, the signal is split into four new signals. Each new signal is passed through a band pass filter with a slightly different center frequency. This process ensures that the signals, which are collected from the same volume of plasma, are separated in frequency space so that two of the new signals can be correlated with one another to yield turbulent electron temperature fluctuations as described in section 3.2.3. The individual signals then pass through high pass filters, which remove the non-fluctuating part of the signal.

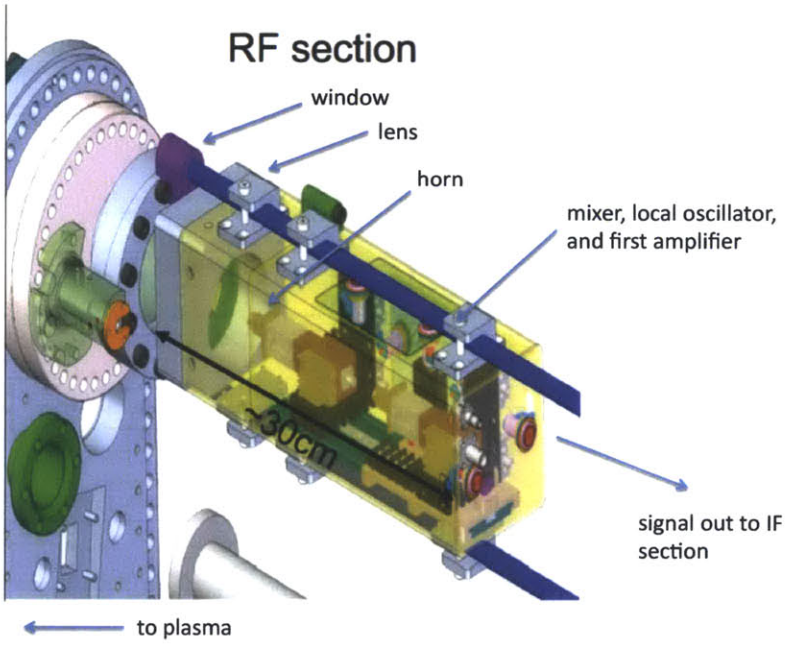

Figure 4-5: The RF section is mounted to the wall of the tokamak. The plasma is to the left of the figure and the emitted radiation passes through the window to the lens. The radiation is collected by the horn antenna and downconverted by a mixer and local oscillator. The signal then passes through an amplifier and is sent to the IF section of the CECE system.

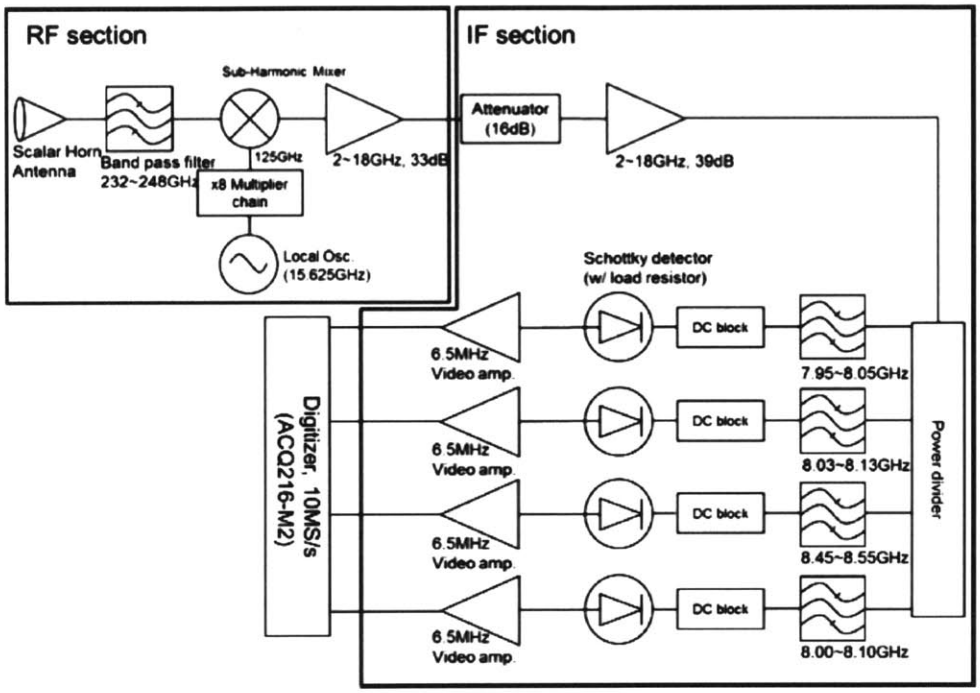

Figure 4-6: Block Diagram of RF and IF sections. The signal from the plasma is collected by the horn antenna in the RD section, downconverted to lower frequencies, and sent to the IF section. In the IF section it is split into four channels that have band pass filters with different center frequencies.

After passing through a video amplifier, each signal is then stored in a database by the digitizer.

4.4 Updated CECE IF section

In future iterations of the CECE diagnostic the design in Figure 4-7 will be implemented. The IF section will be expanded from four to eight channels. This will allow the diagnostic to collect more data during each plasma shot than at present. Additionally, two of the band pass filters will use YIG (yttrium iron garnet) filters. The center frequency of these band pass filters is changed by modifying the magnetic fields around them; using YIG filters enables the CECE diagnostic to collect data using different slices of frequency space without having to open the system and change the hardware. All that needs to be done is to change the magnetic fields surrounding the filters, via a current tuning circuit.

4.5 High Pass Filtering

High pass filters were built and installed in the IF section of the CECE hardware. They were made to have a cutoff frequency of 100 Hz and the voltage response of the four filters is given by Figure 4-8. The filters each use a 1 MΩ resistor in parallel with a 1.5 nF capacitor.

The raw signal collected by the CECE radiometer is given by Figure 4-9 (a). Figure 4-9 (b) gives the signal after the high pass filter has been added to the system. It is clear in this case that the direct current, or non-fluctuating, part of the signal is removed by the high pass filter. This is important because after the non-fluctuating part of the signal is removed, only the fluctuating part remains. This signal is then comprised of the fluctuations due to thermal noise and due to electron temperature fluctuations. As Figure 4-9 shows, the non-fluctuating part of the signal has been removed, making it ready for the cross-correlation technique that yields the data about electron temperature fluctuations in the plasma.

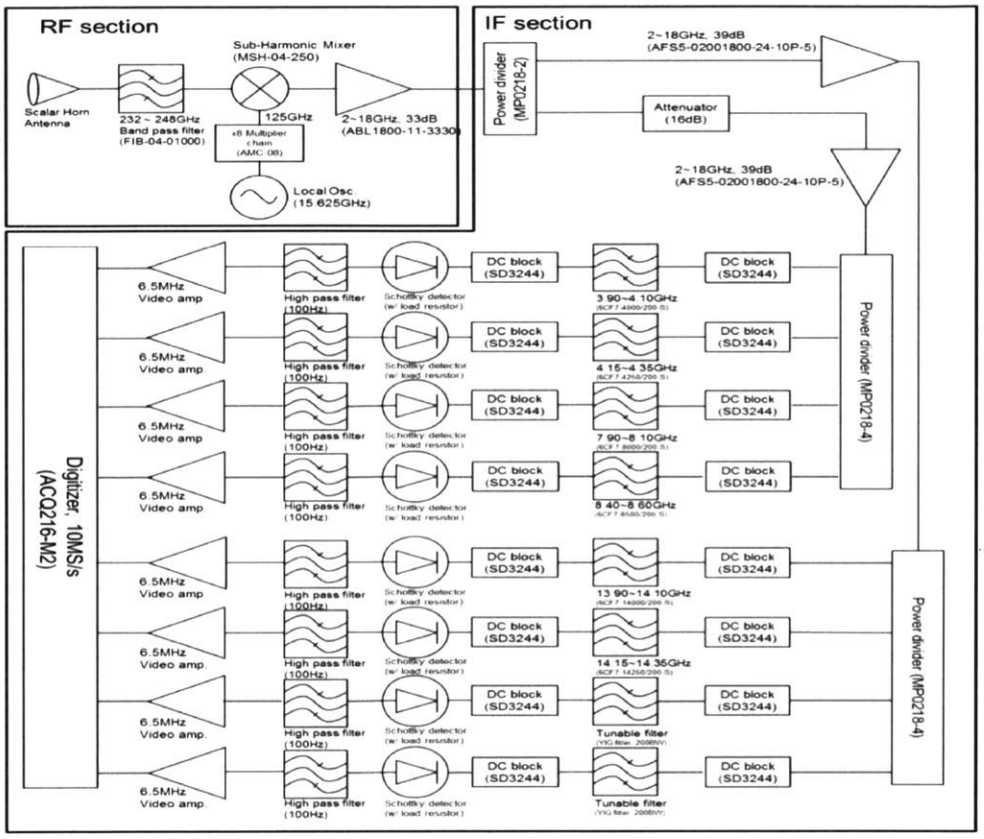

Figure 4-7: Radiometer block diagram with updated IF section. The RF section is the same as in Figure 4-6 but the IF section has been expanded to include eight channels, two of which contain tunable Yttrium Iron Garnet (YIG) filters.

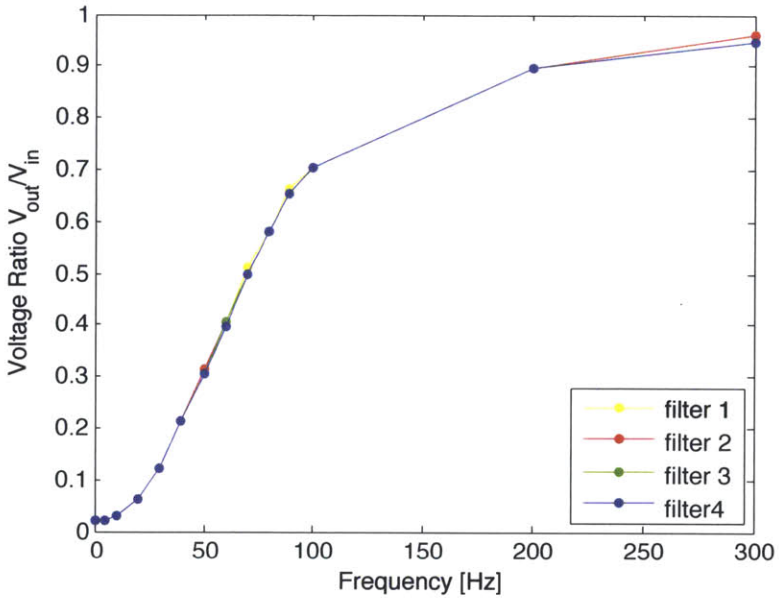

Figure 4-8: Response of the four 100Hz high pass filters built for CECE hardware. The response of the four filters is almost identical and the filters match their intended 3dB frequency of 100Hz well.

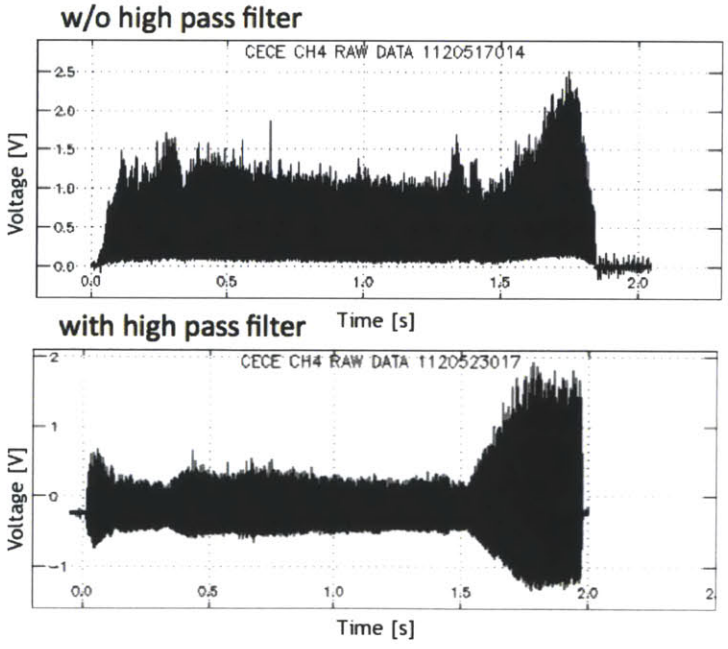

Figure 4-9: Raw CECE signal without the high pass filters (a) and with the high pass filters (b). The high pass filters remove the baseline direct current (DC) signal.

4.6 IDL Codes

Two IDL codes were written during this study: one for a notch filter, which can remove spikes in the data at one frequency, and another for a high pass filter, which allows only parts of the signal with frequency over a cutoff frequency to pass.

The results of the implementation of the notch filter (Appendix A.2) can be seen in Figures 4-10(a) and 4-10(b). The signal is unaffected at frequencies above and below the notch filter frequency.

The high pass filter (Appendix A.1) is successful at removing parts of the signal below the chosen cutoff frequency. Figures 4-11(a) and 4-11(b) show the signal before and after implementing the high pass filter using a cutoff frequency of 10kHz.

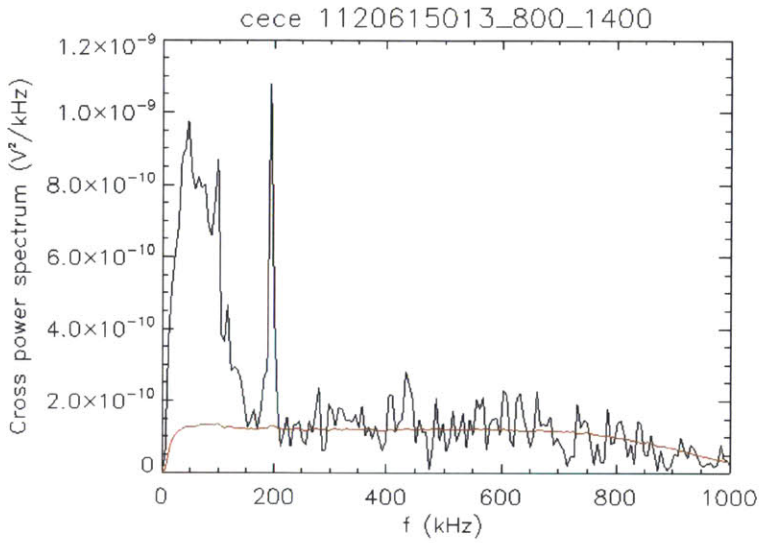

(a) Cross power spectrum without notch filter.

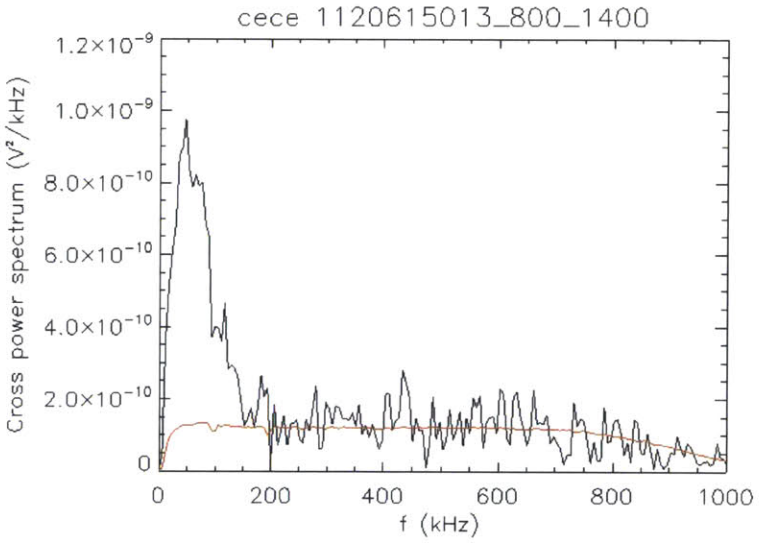

(b) Cross power spectrum with notch filter.

Figure 4-10: Cross power spectrum without a notch filter (a) and with a notch filter (b) applied. The notch filter removes electronics noise at specific frequencies. In this example the notch filter removes peaks at 97.5kHz and 195kHz. These figures were produced using shot 1120615013 integrated between 800 and 1400 ms for channels 1 and 2. The red line indicates the variance of the cross power.

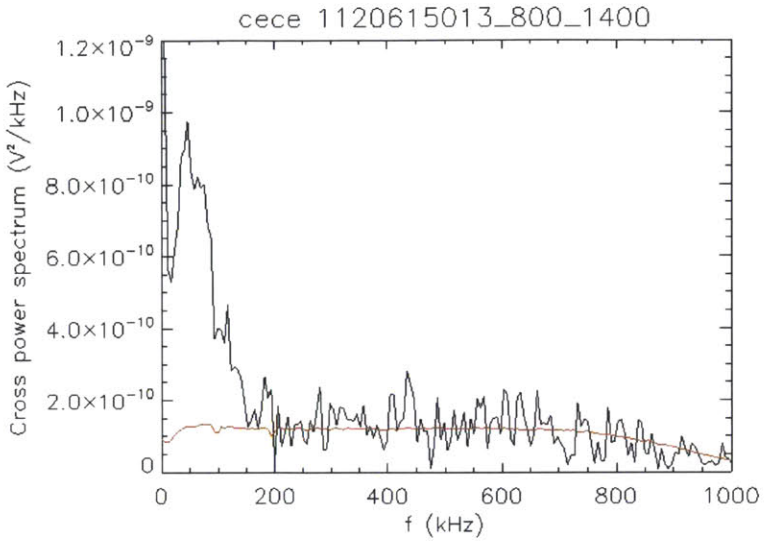

(a) Cross power spectrum without high pass filter.

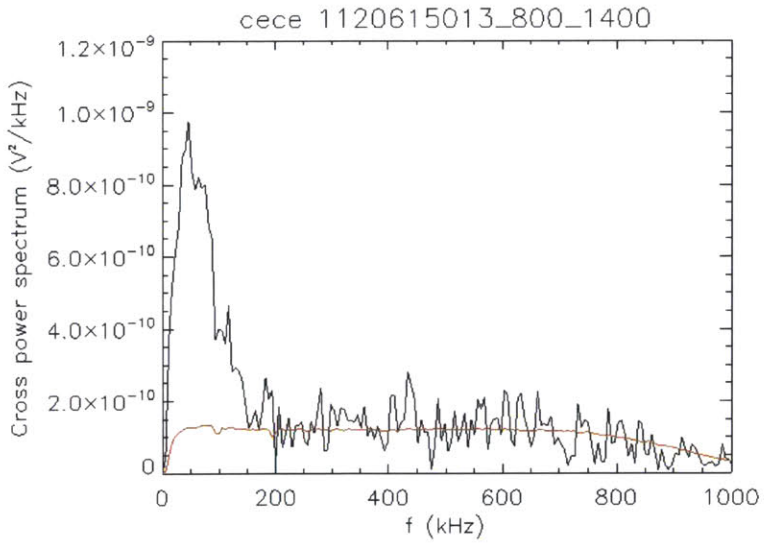

(b) Cross power spectrum with high pass filter.

Figure 4-11: Cross power spectrum without a high pass filter (a) and with a high pass filter (b) applied. The high pass filter removes low frequencies which do not contribute to the electron temperature fluctuations in the signal. These figures were produced using shot 1120615013 integrated between 800 and 1400 ms for channels 1 and 2. The red line indicates the variance of the cross power.

5. Data and Results

5.1 Fluctuations in LOC and SOC

Electron temperature fluctuation data were collected using the CECE radiometer during the summer 2012 run campaign at Alcator C-Mod. The following data were collected from ohmic plasmas. Figure 5-1 shows the relative electron temperature fluctuation level as a function of time in four plasmas. Two of the plasmas (1120615015 and 1120615022) operate in the LOC regime and two of them (1120615025 and 1120615026) operate in the SOC regime. The points were picked at 100ms intervals and the purpose was to get fluctuation levels for short time ranges between 0.5 and 1.5 seconds in order to determine whether the fluctuation levels were higher in LOC throughout the discharge or only when integrated over the entire discharge.The trend in Figure 5-1 shows that the fluctuation levels in the LOC plasmas are higher throughout the shot, which makes sense because the discharges are very stationary; there are no changes in profiles or gradients that would change the drive for the turbulence and no change in turbulence suppression terms, like E×B shear. Table 5.1 gives the plasma parameters for the shots used in Figure 5-1.

Figure 5-2 presents data from ohmic plasmas. Three of the shots fall in the SOC

Shot	ρ ch 1&2	I_p [MA]	B_t [T]	navg [10^{20} m^{-3}]	<n_e> [10^{20} m^{-2}]
1120615022	0.84	1.02	5.45	1	0.56
1120615015	0.84	1.02	5.45	0.75	0.45
1120615025	0.84	1.03	5.45	1.3	0.75
1120615026	0.84	1.03	5.45	1.35	0.8

Table 5.1: Plasma parameters for shots in Figure 5-1

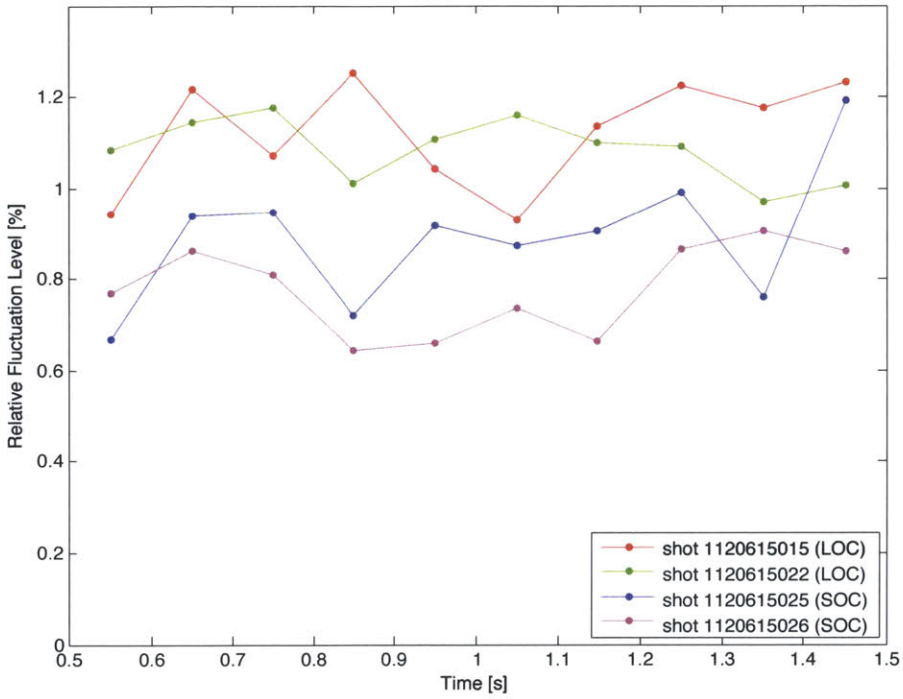

Figure 5-1: Fluctuation time series for LOC and SOC plasmas. The shots used in this figure were all collected at $I_p \sim 1$MA, $B_t \sim 5.45$T, at a location of $\rho \sim 0.84$ for channels 1&2 of the CECE system. The data for the fluctuation levels calculated via cross-correlation of channels 1&2 are shown. The data for the shots used are given in Table 5.1.

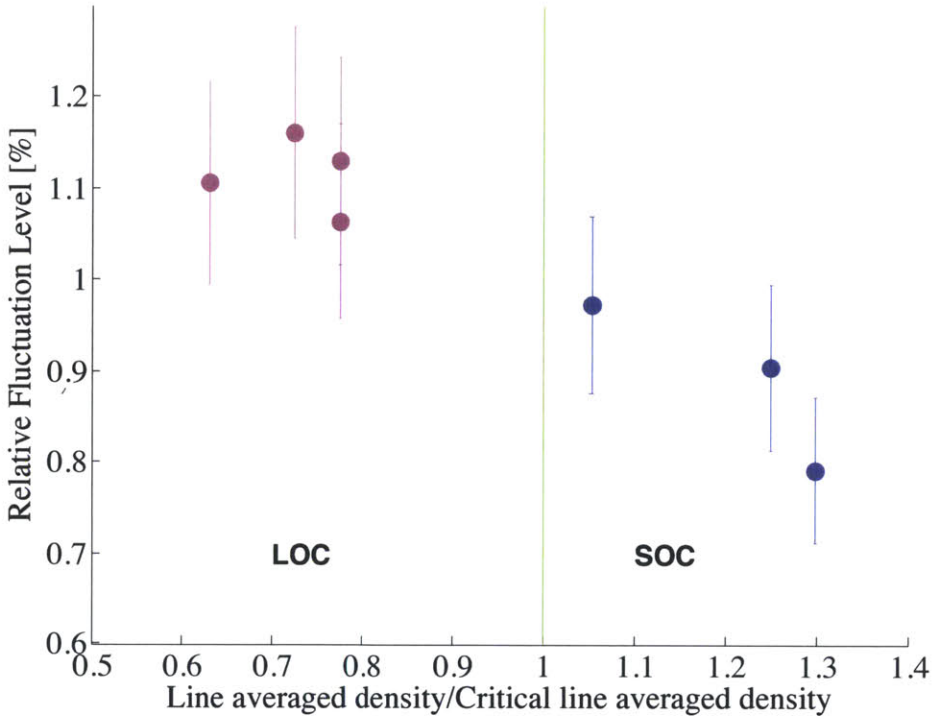

Figure 5-2: Relative fluctuation level as a function of LOC/SOC for shots with $I_p \sim$ 1MA, $B_t \sim$ 5.45T, and $\rho \sim 0.84$ for channels 1&2. Only data from channels 1&2 of the CECE system are shown on the plot. The data for the shots used are given in Table 5.2. The error bars used in this plot have been set to 10%, a value that has been determined via propagation analysis.

regime and four fall in the LOC regime. The demarcation between LOC and SOC occurs when the critical line averaged density is equal to the line averaged density. The critical $<n_e>$ occurs when there is a change in rotation of the plasma, which is correlated to the change in confinement regime between LOC and SOC [3]. The trend seen in Figure 5-2 is that the relative fluctuation level is lower in SOC than in LOC.

Table 5.2 gives the plasma parameters for the shots used in Figure 5-2. All the shots are from the same place in the plasma, corresponding to $\rho \sim 0.84$, have plasma current $I_p \sim 1$ MA, and were run at a magnetic field of $B_T \sim 5.45$ T. The major varying parameter between the seven shots is the density. The shots are arranged with the lowest density shots on the far left of the plot and track right with increasing density.

Shot	ρ ch 1&2	I_p [MA]	B_t [T]	navg [10^{20} m^{-3}]	<n_e> [10^{20} m^{-2}]	Line averaged density/Critical line averaged density	LOC/ SOC
1120615013	0.84	1.02	5.45	0.65	0.4	0.63	LOC
1120615015	0.84	1.02	5.45	0.75	0.45	0.72	LOC
1120615017	0.84	1.02	5.45	0.8	0.45	0.78	LOC
1120615021	0.84	1.02	5.49	0.8	0.45	0.78	LOC
1120615024	0.84	1.03	5.45	1.1	0.65	1.05	SOC
1120615025	0.84	1.03	5.45	1.3	0.75	1.25	SOC
1120615026	0.84	1.03	5.45	1.35	0.8	1.30	SOC

Table 5.2: Plasma parameters for shots in Figure 5-2

5.2 Linear Stability Analysis

Figures 5-3(a) and 5-3(b) show the linear stability analysis done for CECE plasmas in the LOC and SOC regimes. This analysis was conducted using linear GYRO simulations. The range $k_y\rho_s \leq 0.3$ is considered in this analysis because this is the range in which CECE measurements can be made. The left plots in Figures 5-3(a) and 5-3(b) show the real frequency (ω_r) of the dominant turbulence mode. A positive real frequency ω_r indicates electron mode turbulence is dominant and a negative real frequency ω_r indicates that ion mode turbulence is dominant.

As indicated by Figure 5-3(a), the electron mode is dominant in the LOC plasma because the real frequency ω_r is positive in the shaded region where CECE is able to make measurements. In Figure 5-3(b) the case is less clear, because ω_r is negative in the region $k_y\rho_s \leq 0.3$ but it increases to be greater than zero for $k_y\rho_s \geq 0.6$. This indicates that in the region where CECE makes measurements, the ion mode is dominant for SOC plasmas. It is possible that the electron mode is connected to TEM turbulence and the ion mode is connected to ITG turbulence; this may indicate that the broadband fluctuations measured by CECE come from TEM driven turbulence in LOC plasmas and shift to ITG driven turbulence in SOC plasmas. The linear growth rates (γ) of the dominant turbulence modes are given by the right plots in Figures 5-3(a) and 5-3(b).

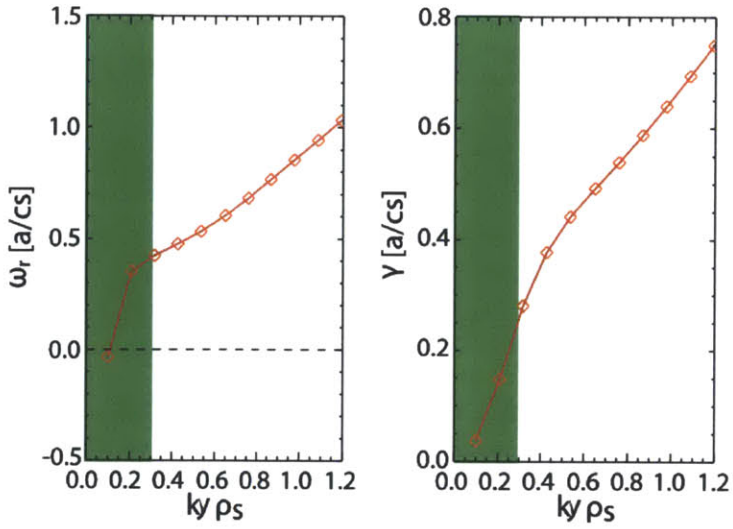

(a) Linear stability analysis LOC plasmas.

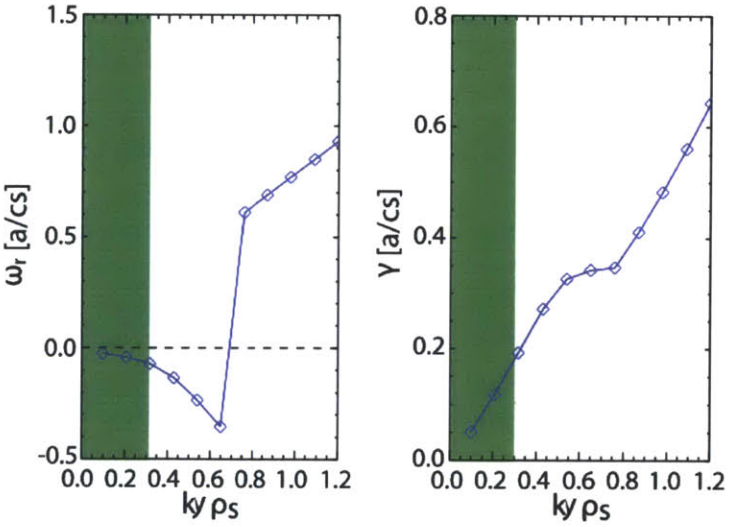

(b) Linear stability analysis SOC plasmas.

Figure 5-3: Figure 5-3(a) shows linear stability analysis for LOC plasmas (shot 1120626023) and Figure 5-3(b) does the same for SOC plasmas (shot 1120626028). The horizontal axis for both figures is $k_y\rho_s$, where k_y is the poloidal wavenumber of the turbulence and ρ_s is the main ion's Larmor radius. The left plots show the real frequency (ω_r) of the dominant turbulence modes. Both vertical axes are in terms of a/c_s, where a is the minor radius of the plasma and c_s is the ion sound speed. Positive ω_r indicates electron mode turbulence and negative ω_r indicated ion mode turbulence. The shaded area ($k_y\rho_s \leq 0.3$) gives the CECE measurement region.

6. Conclusion

6.1 Discussion

The data presented in this thesis has shown that CECE observes lower levels of electron temperature fluctuations in the SOC regime than in the LOC regime. This runs counter to the line-averaged density fluctuation data collected from ohmic plasmas in past experiments. It is, however, not inconsistent with these results because they measured line-averaged density fluctuations, while the CECE diagnostic at Alcator C-Mod measures local electron temperature fluctuations.

The apparent contradiction between those results that measured higher density fluctuations in the SOC regime and lower density fluctuations in the LOC and the results obtained via CECE at Alcator C-Mod can be explained by the dominant turbulence modes in each confinement regime. Linear stability analysis has shown that the LOC regime is dominated by TEM turbulence and the SOC regime is on the border between the ITG and TEM turbulence modes being dominant. It is reasonable to believe that the TEM turbulence mode drives large electron temperature fluctuations [18], which explains the higher electron temperature fluctuation levels seen in the LOC regime compared to the SOC regime.

6.2 Future Work

The CECE data collected at Alcator C-Mod to date has been localized around ρ of about 0.8-0.9. Future work on the system will involve adjusting the radiometer's optical system to see further inside the plasma. This will provide a picture of the

radial dependence of the phenomena explored in this thesis.

A. IDL Programs

A.1 High Pass Filter IDL Program

```
function hpf,signal,T,cutoff_freq

;y : data or signal to be filtered
;T : total time period [s]
;cutoff_freq : cutoff frequency [Hz]
;same as lpf except flip cutoff_freq/fre_sig in filter

num_ch=n_elements(signal)

pos_fre_sig=findgen(num_ch/2+1)/(T)
neg_fre_sig=-reverse(findgen(num_ch/2-1)+1)/(T)
fre_sig=[pos_fre_sig,neg_fre_sig]
fre_num_sig=sort(fre_sig)


butter_n=5
filter=1/(1+(cutoff_freq/fre_sig)^(2*butter_n))

y = fft( fft( signal , -1 ) * filter, 1 )

return,y
```

```
end
```

A.2 Notch Filter IDL Program

```
function notchf,signal,f_notch,fft_num

;f_notch: frequency of the notch
;T: total time period [s]

delt = 0.2
c = (1.0-!PI*f_notch*delt) / (1.0+!PI*f_notch*delt)
b = [(1+c^2)/2, -2*c, (1+c^2)/2]
a = [c^2, -2*c, 1]

width = 1.5
;change the width of the filter depending on the fft window size
if fft_num lt 60000 then begin
width = 1.5 ;parameter to control how broad the peak suppression is
endif
if fft_num lt 17000 then begin
width = 2
endif
if fft_num lt 5000 then begin
width = 3
endif
start = int(f_notch*2.048)-width*512 ;index at which notch filter begins acting

na = n_elements(a)-1
nb = n_elements(b)-1
```

```
N = 1024L
U = fltarr(N)
U[0] = float(N)
Y = fltarr(N)
Y[0] = b[2]*U[0]/A[na]

;generates an array of coefficients that can be used to effectively dull certain frequencies
for k=1,N-1 do $
Y[k] = (total(b[nb-k>0:nb]*U[k-nb>0:k]) $
- total(a[na-k>0:na-1]*Y[k-na>0:k-1])) / a[na]

Ybig = findgen(n_elements(Y)*width) ;expand the array of coefficients to broaden effect
for i=0,n_elements(Y)*width-1 do Ybig[i] = Y(i/width) ;expand array
v = fft(Ybig)
filter = make_array(n_elements(signal),1, /integer, value = 1) ;make an array of ones
filter[start:start+width*1024-1] = abs(v(0:N*width-1)) ;replace some ones with smaller coefficients

z = fft( fft( signal , -1 ) * filter, 1 ) ;get new signal
z = fft( fft( z , 1 ) * filter, -1 ) ;necessary because data folds over (or shifts?) so need to apply filter twice

return, z
end
```

Bibliography

[1] R. A. et al., "The ITER design," *Plasma Phys. Control. Fusion*, vol. 44, pp. 533–537, 2002.

[2] J. Freidberg, *Plasma Physics and Fusion Energy.* Cambridge University Press, 2007.

[3] J. E. R. et al., "Rotation Reversal Bifurcation and Energy Confinement Saturation in Tokamak Ohmic L-Mode plasmas," *PRL*, vol. 107, pp. 265001–4, 2011.

[4] C. Bourdelle, "Turbulent Particle Transport in Magnetized Fusion Plasma," *Plasma Phys. Control. Fusion*, vol. 47, pp. A317–A325, 2005.

[5] C. A. et al., "Relationship Between Density Peaking, Particle Thermaldiffusion, Ohmic Confinement, and Microinstabilities in ASDEX Upgrade L-Mode Plasmas," *Phys. Plasma*, vol. 040701, pp. 1–4, 2005.

[6] B. E. et al., "Transport Analysis of Ohmic, L-Mode and Improved Confinement Discharges in FTU," *Plasma Phys. Control. Fusion*, vol. 46, pp. 1793–1804, 2004.

[7] L. L. et al., "Studies of Turbulence and Transport in Alcator C-Mod Ohmic Plasmas with Phase Contrast Imaging and Comparisons with Gyromagnetic Simulations," *Plasma Phys. Control. Fusion*, vol. 51, pp. 3, 9, 15–16, 2009.

[8] C. L. R. et al., "Appearance of a Low-Frequency Turbulence Feature During Saturated Ohmic Confinement Discharges," *Plasma Phys. Control. Fusion*, vol. 43, pp. 1273–1280, 2001.

[9] J. Candy and R. E. Waltz, "The Local Limit of Global Gyrokinetic Simulations," *Phys. Plasma*, vol. 11, pp. L25–L27, 2004.

[10] J. Wesson, *Tokamaks.* Oxford University Press, 1987.

[11] A. G. Lynn, *Electron Cyclotron Emission Measurements of Coherent and Broadband Density Fluctuations in the Alcator C-Mod Tokamak.* PhD thesis, University of Texas at Austin, 2004.

[12] B. B. Kadomtsev, *Tokamak Plasma: A Complex Physical System.* Institute of Physics Pub., 1992.

[13] I. Hutchinson, *Principles of Plasma Diagnostics.* Cambridge University Press, 2 ed., 2002.

[14] G. B. Rybicki and A. P. Lightman, *Radiative Processes in Astrophysics.* John Wiley & Sons, 1979.

[15] A. E. W. et al., "A Correlation Electron Cyclotron Emission Diagnostic and the Importance of Multifield Fluctuation Measurements for Testing Nonlinear Gyrokinetic Turbulence Simulations," *Rev. Sci. Instrum.*, vol. 79, p. 103505, 2008.

[16] C. W. et al., "Comparison of Different Methods of Electron Cyclotron Emission-Correlation Radiometry for the Measurement of Temperature Fluctuations in the Plasma Core," *Rev. Sci. Instrum.*, vol. 75, p. 3177, 2004.

[17] C. S. et al., "Design of a Correlation Electron Emission Diagnostic for Alcator C-Mod," *Rev. Sci. Instrum.*, vol. 83, p. 10E311, 2012.

[18] A. E. W. et al., "Simultaneous measurement of core electron temperature and density fluctuations during electron cyclotron heating on DIII-D," *Phys. Plasma*, vol. 17, p. 020701, 2010.